ESC European Society of Cardiology

Europace (2025) **27**, euaf099
https://doi.org/10.1093/europace/euaf099

Translational approach to ventricular innervation: the posterior descending ganglionated plexus

Ann-Kathrin Kahle [1,2,3], Niklas Klatt[3,4], Katharina Scherschel [1,3,5,6], Christiane Jungen [3,7], Pawel Kuklik [8], Fares-Alexander Alken [1,3], Nikolaj Klöcker [5,6], Stephan Willems [3,8], Elvira Weber [6,9,10], Udo Boeken [6,9], Artur Lichtenberg [6,9], Alexander Bernhardt [11], Samer Hakmi[12], Dainius H. Pauza[13], and Christian Meyer [1,3,5]*

[1]Division of Cardiology, Angiology, Intensive Care Medicine, EVK Düsseldorf, cNEP, cardiac Neuro- and Electrophysiology Research Consortium, Kirchfeldstrasse 40, 40217 Düsseldorf, Germany; [2]Department of Cardiology, Pulmonology and Vascular Medicine, Medical Faculty and University Hospital Düsseldorf, Heinrich Heine University, Moorenstrasse 5, 40225 Düsseldorf, Germany; [3]DZHK (German Centre for Cardiovascular Research), Partner Site Hamburg/Kiel/Lübeck, Potsdamer Strasse 58, 10785 Berlin, Germany; [4]Department of Cardiology, Schön Klinik Neustadt in Holstein, Am Kiebitzberg 10, 23730 Neustadt in Holstein, Germany; [5]Institute of Neural and Sensory Physiology, cNEP, cardiac Neuro- and Electrophysiology Research Consortium, Heinrich Heine University Düsseldorf, Medical Faculty, Universitätsstrasse 1, 40225 Düsseldorf, Germany; [6]Cardiovascular Research Institute Düsseldorf (CARID), Medical Faculty and University Hospital Düsseldorf, Heinrich Heine University, Moorenstrasse 5, 40225 Düsseldorf, Germany; [7]Department of Cardiology and Vascular Medicine, West German Heart and Vascular Center, University Hospital Essen, University Duisburg-Essen, Hufelandstrasse 55, 45147 Essen, Germany; [8]Department of Cardiology and Internal Intensive Care Medicine, Asklepios Hospital St. Georg, Lohmühlenstrasse 5, 20099 Hamburg, Germany; [9]Department of Cardiac Surgery, Medical Faculty, University Hospital Düsseldorf, Moorenstrasse 5, 40225 Düsseldorf, Germany; [10]Research Group 3D Cardiovascular Regenerative Medicine and Tissue Engineering (CURE 3D), Department of Cardiac Surgery, Medical Faculty, University Hospital Düsseldorf, Heinrich-Heine-University Düsseldorf, Moorenstrasse 5, 40225 Düsseldorf, Germany; [11]Department of Cardiovascular Surgery, University Heart and Vascular Center Hamburg, Martinistrasse 52, 20246 Hamburg, Germany; [12]Department of Cardiovascular Surgery, Asklepios Hospital St. Georg, Lohmühlenstrasse 5, 20099 Hamburg, Germany; and [13]Institute of Anatomy, Lithuanian University of Health Sciences, A. Mickeviciaus g. 9, 44307 Kaunas, Lithuania

Received 19 February 2025; accepted after revision 1 May 2025; online publish-ahead-of-print 13 May 2025

Aims

Modulation of cardiac neural control is increasingly explored to treat cardiac arrhythmias. While the atrially located ganglionated plexus (GPs) have been studied intensively, characterization of ventricular GPs is sparse. This proof-of-principle study aimed to assess the role of the posterior descending GP (PDGP) for neural control of cardiac electrophysiology, while offering a translational roadmap into clinical practice.

Methods and results

Since an initial systematic literature review revealed the PDGP as a small, consolidated GP on the posterior left ventricle (LV) in dogs, swine, and humans, we subsequently conducted morphological C57BL/6 murine studies ($n = 43$) indicating ventricular GPs in only 10% of hearts. Based on our initial findings, in a proof-of-principle study analysing 4300 local unipolar electrograms from a multi-electrode sock, the impact of functional PDGP modulation was studied in an *ex vivo* retrograde-perfused porcine model. Wave propagation characteristics determined by epicardial activation mapping demonstrated increased dispersion of conduction velocity during high-frequency (8.52 ± 2.24 radian vs. 2.79 ± 0.89 radian; $P = 0.018$) and nicotine stimulation (19.79 ± 6.49 radian vs. 2.79 ± 0.89 radian; $P = 0.044$) compared to paced rhythm. High-frequency stimulation prolonged activation recovery intervals in the posterior (257.8 ± 6.7 ms vs. 244.8 ± 1.9 ms; $P = 0.044$) and basal (258.1 ± 4.2 ms vs. 244.8 ± 1.9 ms; $P = 0.039$) right ventricle compared to the posterior LV. Analysis of explanted human hearts confirmed the presence of the PDGP within epicardial adipose tissue near its eponymous coronary artery and the posteromedial left atrial GP. Three-dimensionally reconstructed human hearts suggested the PDGP localization characterized by inter-patient anatomical variability.

* Corresponding author. Tel: +49 211 919 1855; fax: +49 211 919-3900. *E-mail address:* christian.meyer@evk-duesseldorf.de

Conclusion The present translational approach to ventricular innervation demonstrates first evidence of the functional relevance of the PDGP, with morphological findings indicating species-related differences. Novel imaging modalities might pave the way for future functional and therapeutic interventions.

Graphical Abstract

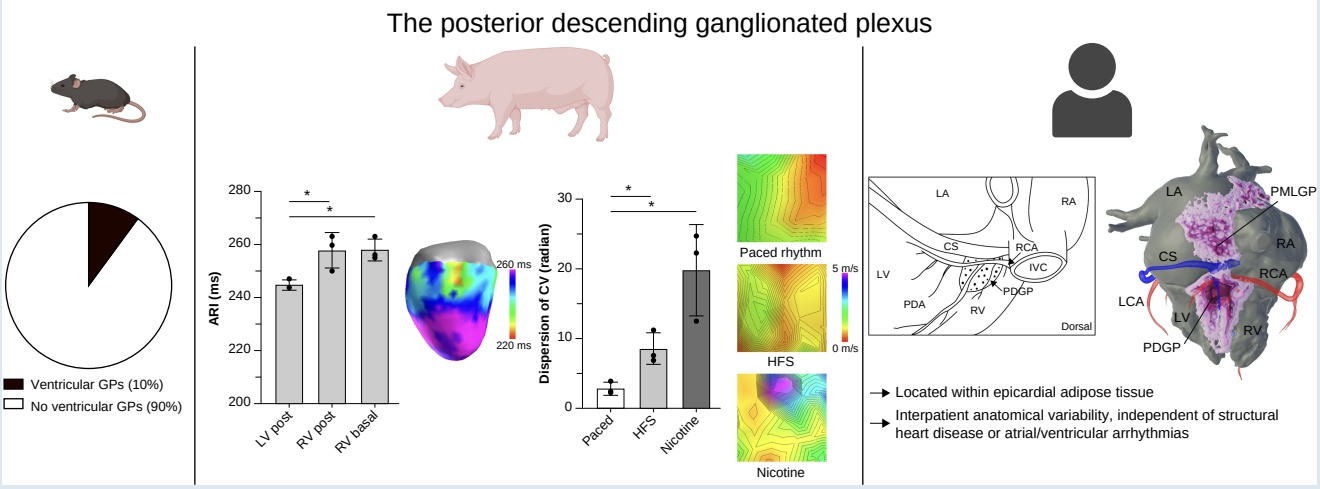

Translational findings on the PDGP from mice to men are illustrated. The present translational approach to ventricular innervation demonstrates first evidence of the functional relevance of the PDGP located within epicardial adipose tissue, with morphological findings indicating that important species-related differences might exist. The close proximity to the posteromedial left atrial GP in humans should be considered during cardioneuroablation procedures. ARI, activation recovery interval; CS, coronary sinus; CV, conduction velocity; GP, ganglionated plexus; HFS, high-frequency stimulation; IVC, inferior vena cava; LA, left atrium; LCA, left coronary artery; LV, left ventricle; PDA; posterior descending coronary artery; PDGP, posterior descending ganglionated plexus; PMLGP; posteromedial left atrial GP; RA, right atrium; RCA, right coronary artery; RV, right ventricle.

Keywords GP stimulation • Intrinsic cardiac nervous system • Posterior descending GP • Swine model • Ventricular electrophysiology

What's new?

- The posterior descending ganglionated plexus (PDGP) is a small, consolidated ventricular GP located on the posterior side of the left ventricle close to the ostium of the coronary sinus and the origin of the posterior descending coronary artery.
- Species-dependent differences considering the presence of the PDGP exist, with ventricular GPs being present in only 10% of C57BL/6 murine hearts.
- In this proof-of-principle study using an *ex vivo* porcine model, PDGP high-frequency and local nicotine stimulation increase the dispersion of conduction velocity, while PDGP high-frequency stimulation evokes regional differences in activation recovery intervals.
- The PDGP is regularly present in human hearts located at the septum within epicardial adipose tissue and near its eponymous coronary artery suggesting that acute and chronic changes in autonomic function might be related to cardiac arrhythmogenesis.
- Three-dimensionally reconstructed human hearts suggest the localization of the PDGP which is characterized by inter-patient anatomical variability.
- The role of the PDGP needs to be considered during cardioneuroablation procedures targeting the posteromedial left atrial GP, which is located in close proximity.

Introduction

The autonomic nervous system is important for the regulation of cardiac electrophysiology and the pathogenesis of arrhythmias.[1] Following the developing mechanistic knowledge on the intrinsic cardiac autonomic nervous system,[2–4] various approaches of neuromodulation are increasingly explored. These global as well as selective strategies often targeting ventricular innervation are used nowadays to treat several patient populations including those with reflex syncope, atrioventricular block, and ventricular tachyarrhythmias.[5,6] However, distinct understanding of functional cardiac neuroanatomy with a focus on ventricular innervation and translation into clinical practice is still necessary.

The network of various clusters of cardiac autonomic ganglia, known as ganglionated plexus (GPs), is a major contributor to intra-cardiac reflexive neural control and cardiac electrophysiology. These GPs consist of cholinergic neurons, some adrenergic neurons, inter-neurons and glial cells, and are associated with sympathetic fibres.[7,8] They function as integration centres for modulation of autonomic inter-actions between the extrinsic and intrinsic cardiac nervous system. Whereas few reports suggested myocardial GPs,[7,8] they are mainly embedded in epicardial fat pads and multiple afferent and efferent nerve fibres project towards the atrial and ventricular myocardium creating a dense neural network.[6,9–11]

The atrially located GPs have been studied in several species.[2,12,13] This pioneering work deepened our physiological understanding of cardiac neural control and paved the way for several novel therapeutic approaches, which are currently under investigation. The atrial GPs are now well known as a 'gatekeeper' integrating autonomic innervation to the sinoatrial and atrioventricular node.[14] As they are mainly located circumferentially around the pulmonary veins, they have been found to be affected by pulmonary vein isolation resulting in partial vagal denervation.[15,16] These changes to cardiac autonomic control can be assessed by functional measurements including an acute heart rate increase as well as release of the neuronal injury marker S100B.[17,18] Furthermore, atrial GPs are commonly targeted during cardioneuroablation procedures, which are emergingly performed in patients with reflex syncope and therefore of increasing interest nowadays.[19–21] However, the long-term effects of accidental or therapeutical atrial GP modulation are still unknown.

Importantly, characterization of ventricular GPs is sparse. In recent years, Pauza *et al.* illustrated the distribution and quantity of epicardiac ventricular GPs in various species laying the cornerstone for subsequent analyses.[22,23] Initially described by some but not all groups,[12,24,25] the posterior descending GP (PDGP) has been found to be a small, consolidated ventricular GP located on the posterior side of the left ventricle (LV) adjacent to the posterior descending coronary artery (PDA). Its potential vascular accessibility suggests the PDGP as a target of clinical interest possibly contributing to the understanding of neurally mediated ventricular arrhythmias. Based on these findings, which, however, underline that this aspect of cardiac neuroanatomy with a focus on ventricular innervation is not entirely explored so far, we hypothesized that the PDGP modifies ventricular electrophysiology and that its neural myocardial control can be altered by electrical high-frequency (HFS) and local nicotine stimulation. Therefore, the present translational approach to ventricular innervation involved a systematic literature review and morphological investigations of the PDGP performed in murine, porcine, and human hearts. Based on our initial findings, an *ex vivo* retrograde-perfused porcine model was developed, and in a proof-of-principle study, the impact of functional PDGP modulation was studied.

Methods

Systematic literature review

We first performed a systematic literature review to determine the presence and location of ganglia in the PDGP area and the effect of ventricular GPs on atrial and ventricular electrophysiology in different species. The literature search was conducted using the terms 'posterior descending ganglionated plexus' OR 'dorsal septal ganglionated plexus' OR 'dorsal interventricular ganglionated plexus' OR 'ventricular ganglionated plexus' in PubMed/MEDLINE. We supplemented our database searches with manual searches of the reference lists of published studies. Potentially eligible studies were assessed independently by two investigators (A.K.K. and C.M.). Studies were included if they covered (i) the PDGP in humans; (ii) the corresponding ventricular GP found at the same location in other species; (iii) ganglia in the PDGP area; or (iv) characterization of the effects of ventricular GPs on atrial and/or ventricular electrophysiology.

Animal studies

All animals were handled in accordance with the institutional guidelines and experiments were registered (ORG_831, 12/2016) by the regional regulatory authorities. The study conforms to the Guide for the Care and Use of Laboratory Animals published by the US National Research Council Committee (8th edition, updated 2011).

Anatomical studies

Innervation of the mouse heart was studied in previous[26,27] and ongoing works conducted by the authors in C57BL/6 mice ($n = 43$, both sexes, 8 to 16 weeks of age). To quantify the presence of ventricular ganglia images from these studies were reviewed by the original investigator. Histology of porcine hearts was conducted as previously described.[26,28] Samples were formalin-fixed for 24–48 h at room temperature, extracted after fixation, dehydrated, paraffin-embedded, and cut into 4 µm sections. Sections were deparaffinized and rehydrated. Haematoxylin–eosin staining was used for the detection of ganglia in the area of the PDGP.

To study the epicardial neural network in the newborn porcine heart, plexus were revealed by applying the acetylcholinesterase method that was described previously by Pauza *et al.*[29]

Finally, morphological analysis of explanted human hearts was performed.

Ex vivo porcine model

Experiments in this study were performed in three swine (female, 4 to 5 months of age) (*Figure 1A*). Animals were fasted 12 h before the procedure and received an intra-muscular injection of 0.2 mg/kg xylazine (Bayer, Leverkusen, Germany) and 20 mg/kg ketamine (Albrecht GmbH, Aulendorf, Germany) for sedation before anaesthesia was induced with intravenous application of 0.4 mg/kg propofol (B. Braun, Melsungen, Germany) via intubation.[9] Animals were heparinized with 25 000 units. For preparation of the heart–lung machine, an additional 25 000 units heparin were administered into the reservoir and an infusion pump with an insulin–glucose-mixture (B. Braun, Melsungen, Germany) at a rate of 10 mL/h was installed. Animals were euthanized by intravenous administration of a lethal dose of pentobarbital sodium (50 mg/kg). Thoracotomy was performed, the heart was exposed, and the aortic root cannulated. Vent catheters were placed in the LV via the left atrial appendage and in the right ventricle (RV) via the right atrial appendage, and the LV was provided with an external pacer (*Figure 1B* and *C*). Extracorporeal circulation was started after the aorta and caval veins were clamped resulting in a coronary perfusion at 37°C. The retrograde-perfused heart with the two lungs was explanted and connected to a dialysis machine operating throughout the whole procedure.

Epicardial mapping with determination of wave propagation characteristics and activation recovery intervals (ARIs) was performed during paced rhythm with 100 bpm close to the base of the heart in the area of the PDGP, during HFS (200 Hz, 4 mA, and 8 V), nicotine and isoprenaline stimulation. Nicotine (100 µL in 1 mL) was locally injected over 30 s into the PDGP region for specific stimulation. Isoprenaline stimulation (10 mmol in 1 mL) was conducted systemically, until an increase in heart rate of 20% was reached (*Figure 1A*)[30] serving as a control for validation of the operability of the used *ex vivo* model. For differentiation to the posteromedial left atrial GP, the PDGP was identified at the cranial aspect of the dorsal interventricular groove, located surrounding the first centimetre of its eponymous coronary artery (*Figure 1B*).[12,24,25]

Epicardial mapping in swine

First, wave propagation characteristics were determined by epicardial activation mapping with two 64-electrode arrays (EcoFlexMEA36, Multi-Channel Systems, Reutlingen, Germany; inter-electrode distance: 300 µm; 1.8 × 1.8 mm) positioned at both ventricles during epicardial pacing (cycle length 600 ms). Unipolar electrograms were recorded (ME128-FAI-MPA-System, Multi-Channel Systems, Reutlingen, Germany) with a sampling rate of 25 kHz.[26,28] Regarding myocardial fibre orientation, longitudinal, and transversal conduction velocities (CVs) were evaluated by calculating latencies between two electrodes, divided by the inter-electrode distance.[31] CV and dispersion of CV were determined using a dedicated software (EPAS).[32]

Second, a custom-built multi-electrode sock (104 silver electrodes, electrode size 0.8 mm, spacing 7–10 mm) was placed around the epicardium (*Figure 1C*). CV and ARI measurements during autonomic nervous system manipulation were consistently performed during controlled epicardial ventricular pacing, with two sock electrodes (located on the posterior interventricular part of the epicardium) connected to a stimulus generator (UHS 20, Biotronik, Berlin, Germany), modified from a previously described protocol.[32] The pacing output was set to the double capture threshold. Local unipolar electrograms were recorded (ME128-FAI-MPA-System, Multi-Channel Systems, Reutlingen,

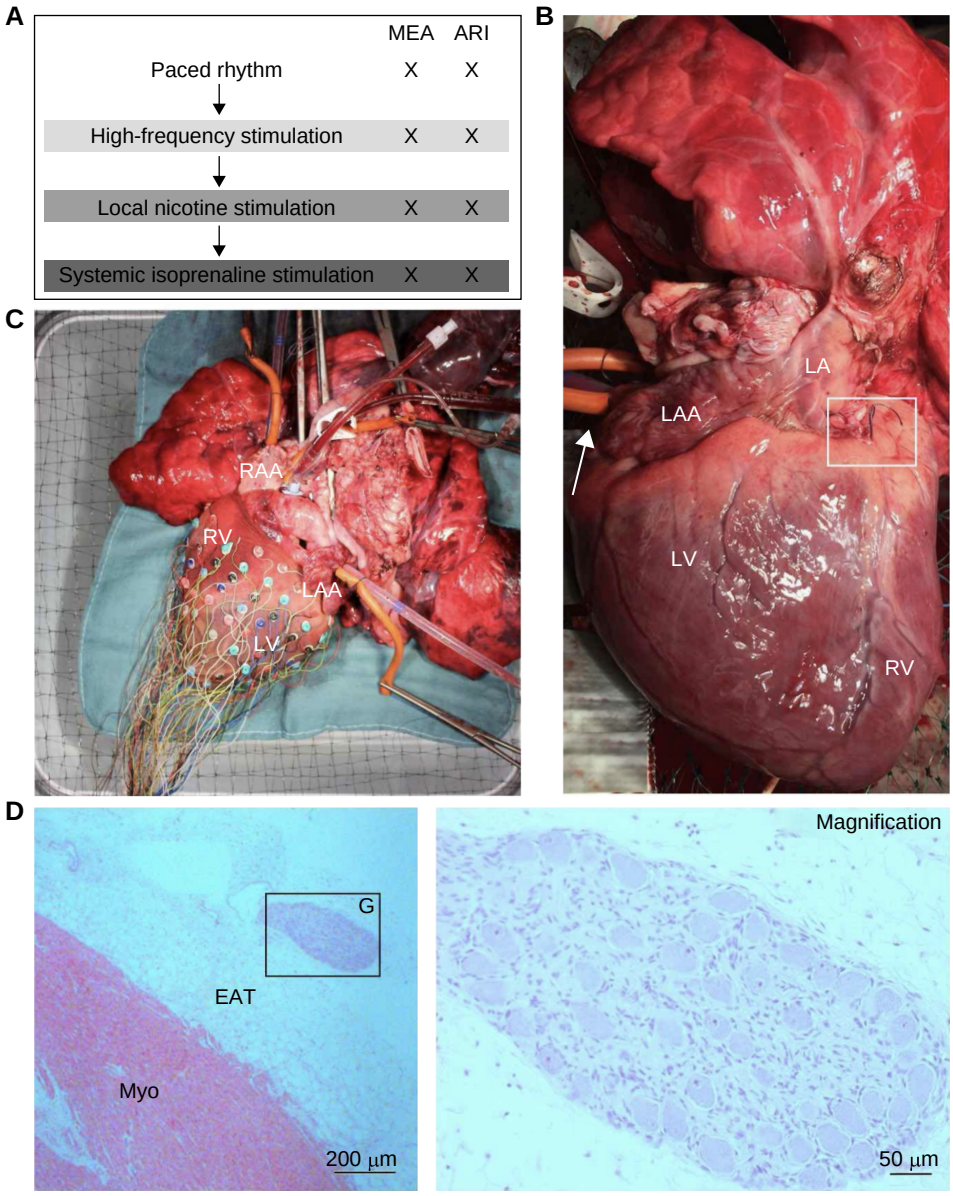

Figure 1 Modification of the PDGP in an *ex vivo* porcine model. (*A*) Study protocol. (*B*) The area of interest including the PDGP located at the septum close to the coronary sinus ostium is marked. One vent catheter was placed in the LV *via* the LAA (white arrow). (*C*) Set-up of the *ex vivo* porcine model consisting of an explanted beating heart with the two lungs connected to a heart–lung machine. (*D*) Haematoxylin–eosin-stained cross section illustrating a ganglion (marked) within the area of the PDGP adjacent to EAT. ARI, activation recovery interval; EAT, epicardial adipose tissue; G, ganglion; LA, left atrium; LAA, left atrial appendage; LV, left ventricle; MEA, multi-electrode activation mapping; Myo, ventricular myocardium; PDGP, posterior descending ganglionated plexus; RAA, right atrial appendage; RV, right ventricle.

Germany) at a sampling rate of 20 kHz. Electrograms were bandstop-filtered (cut-off 200 Hz, bandstop resonator: 50 Hz, Q-factor 2.0) using MC Rack, Version 4.6.2, 2015, Multi-Channel System. For post-procedural analysis, data were imported into a dedicated software (EPAS) and bandpass-filtered (lower 3 Hz and upper 50 Hz) using a third-order Butterworth filter.[32] The ARI as a surrogate parameter for action potential duration was defined as the interval between the maximum negative dV/dt of the activation signal to the maximum positive dV/dt of the repolarization wave.[32] ARIs in all LV and RV areas were compared with each other. Visualization of ARI values using a heatmap was additionally performed by artificial intelligence.

Three-dimensional reconstruction of human hearts

In a series of eight patients, cardiac computed tomography scans were performed.[33] Segmentation (inHEART, Bordeaux, France) resulted in the generation of the four cardiac chambers meshes along with additional meshes used for visualization (aorta and coronary arteries, coronary sinus, phrenic nerve, fossa ovalis, ventricles, oesophagus, and pericardium).[33] Epicardial fat was segmented by identifying voxels in the −300/−10 HU range in immediate proximity with the segmented atria and ventricles (in the vicinity of the pericardium and the cardiac chambers) and fat pads extracted by serial

Table 1 Presence of ganglia in the PDGP area in different species

Study	Species	Results
Tanaka *et al.*, *Anat Rec*, 2007[35]	Mice	• One sympathetic nerve of the branch arising from the sympathetic ganglia at the level of T2–T5 contributes to the plexus of the pulmonary venous sinus and to the middle cardiac vein towards the dorsal wall of the right ventricle.
Rysevaite *et al.*, *Heart Rhythm*, 2011[36]	Mice	• Originating from the left-sided nerves, epicardial nerves proceed onto the dorsal surfaces of the left atrium and both ventricles as the left dorsal neural pathway or sub-plexus.
Yuan *et al.*, *Anat Rec*, 1994[25]	Dogs	• The dorsal septal GP is located adjacent to the dorsal descending coronary artery. • It contains a mean of 17 ± 4 ganglia per heart, with 12.3 ± 2.4 ganglia with <50 neurons, 2.7 ± 0.6 with 50–100, 1.3 ± 0.7 with 100–200 and 0.2 ± 0.2 ganglia with >200 neurons.
Arora *et al.*, *Anat Rec*, 2003[24]	Swine	• The dorsal interventricular GP overlies the cranial aspect of the dorsal interventricular groove, located surrounding the first centimetre of the dorsal interventricular coronary artery. • It contains a mean of 95 neurons and 7 ganglia per heart, with 4 ± 2 ganglia with 1–10 neurons, 2 ± 1 with 11–50 and 1 ± 0.3 ganglia with 51–100 neurons.
Pauziene *et al.*, *Anat Rec*, 2017[22]	Swine	• The right ventricular nerves spread on the ventral and lateral surfaces of the right ventricle turning towards its dorsal surface. • The dorsal ventricular nerves outspread from the left and the middle dorsal neural sub-plexus on the dorsal left atrium. They cross the coronary groove at the coronary sinus and mainly distribute on the dorsal surface of the ventricles, reaching the apex.
Saburkina *et al.*, *Heart Rhythm*, 2010[11]	Sheep	• Epicardial nerves of the middle dorsal sub-plexus pass through the coronary groove and spread onto the dorsal side of both ventricles. • The majority of left dorsal sub-plexal nerves extends onto the dorsal side of both ventricles, accompanied by multiple epicardial ganglia.
Janes *et al.*, *Am J Cardiol*, 1986[4]	Humans	• The major cardiac plexuses contain three large cardiac nerves, the right and left coronary cardiac nerves and the left lateral cardiac nerve, as well as small nerve fibres innervating the ventricles. • The left ventral cardiopulmonary nerve unites with small nerve fibres from the ventral cardiopulmonary plexus and forms the right coronary cardiac nerve projecting onto the heart along the right coronary artery.
Armour *et al.*, *Anat Rec*, 1997[12]	Humans	• The posterior descending GP is a smaller GP associated with the origin of the posterior descending coronary artery. • It contains a mean of 5.2 ± 1.9 ganglia per heart, with 4.1 ± 2.2 ganglia with 5–10 neurons and 1.6 ± 0.6 with 11–50.
Pauza *et al.*, *Anat Rec*, 2000[2]	Humans	• The post-ganglionated nerves of the left coronary sub-plexus supply the ventral, lateral, and, in part, dorsal walls of the left ventricle, as well as the ventral, lateral, and dorsolateral parts of the coronary sulcus. They are more numerous and denser than the ones of the right coronary sub-plexus and on the dorsolateral left ventricular surface, they overlap with the epicardiac nerves extending by the left dorsal sub-plexus. • The majority of the post-ganglionated nerves of the left dorsal sub-plexus passes through the left dorsal coronary sulcus and spreads onto the dorsal surface of the left ventricle.
Saburkina *et al.*, *Anat Rec*, 2023[23]	Humans and sheep	• Atrial epicardiac nerves coming from the venous part of the heart hilum proceed along the diaphragmatic wall of the left atrium, pass the coronary groove and spread on the diaphragmatic surface of both human ventricles. • The sheep ventricles are supplied by atrial epicardial nerves, of which two third extend through the dorsal wall of the left atrium, cross the coronary groove and spread on the dorsal surface of both ventricles as nerves of the left and middle dorsal epicardiac ganglionated nerve sub-plexus. • The mean thickness of the human nerves at the dorsal ventricular surface site is 200 ± 39 μm, while it is 170 ± 14 μm in sheep.

GP, ganglionated plexus.

erosions with 0.5 mm steps (0/0.5/1/1.5/2 mm). Cardiac anatomy and myocardial wall thinning maps were reviewed on a cloud-based Model Explorer. Three-dimensional reconstructions suggested the localization of the PDGP. Anatomical characteristics including its size and relative position towards adjacent anatomical structures were manually measured and analysed by one investigator (A.-K.K.).

Statistical analysis

Data are presented as mean ± SD. The Student's *t*-test and analysis of variance with multiple comparisons were used, as appropriate.[17,34] A *P* value <0.05 was considered statistically significant. All analyses were performed using GraphPad Prism 9.5.1 (GraphPad Inc., La Jolla, CA).

Table 2 Effects of ventricular GPs on atrial and ventricular electrophysiology

Ventricular GP	Species	Stimulation	Atrial effect	Ventricular effect	Comment
CMVGP[37]	Canine	Nicotine	• Bradycardia or tachycardia in 82% • AV block in >30% • AF induction in >35% • Biatrial unipolar wave form changes	• Widespread biventricular wave form changes, with a higher incidence compared to RAGP stimulation	• Ventricular changes occurred concomitantly with the later (adrenergic) phase of the biphasic atrial chronotropic response (i.e. ~90 s after nicotine injection)
VSVGP[37]	Canine	Nicotine	• Bradycardia or tachycardia in 71% • No AV block • No AF induction	Unknown	—
RVGP[37]	Canine	Nicotine	• Bradycardia or tachycardia in 55% • AV block in >30% • No AF induction • Unipolar wave form changes at the right atrial free wall, with a similar distribution as after RAGP stimulation	Unknown	• Atrial changes occurred concomitantly with the early phase (bradycardia) of the biphasic atrial chronotropic response (i.e. ~20 s after nicotine injection)
AoGP[38]	Canine	High-level electrical stimulation	• Decreased atrial and PV ERP • Decreased acetylcholine and isoprenaline threshold concentration for AF • Increased AF inducibility	Unknown	—
		Low-level electrical stimulation	• Prevented shortening of atrial and PV ERP • Increased acetylcholine and isoprenaline threshold concentration for AF • Decreased AF inducibility		
PDGP	Swine	HFS	Unknown	• Increased ARI at the posterior and basal RV compared to the posterior LV • Increased global CV dispersion[a]	—
		Nicotine		• Increased global CV dispersion[a]	
		Isoprenaline		• Increased ARI at the posterior, basal and midventricular RV[a] • Increased ARI at the anterior, posterior, basal and midventricular RV compared to the posterior and basal LV	

AF, atrial fibrillation; AoGP, aortic root GP; ARI, activation recovery interval; AV; atrioventricular; CMVGP, cranial medial ventricular GP; CV, conduction velocity; ERP, effective refractory period; HFS, high-frequency stimulation; LV, left ventricle; PDGP, posterior descending ganglionated plexus; PV; pulmonary vein; RAGP, right atrial GP; RV, right ventricle; RVGP, right ventricular GP; VSVGP, ventral septal ventricular GP.
[a]Compared to pacing.

Results

Presence and location of ganglia in the posterior descending ganglionated plexus area in different species

A systematic literature review revealed the presence of the PDGP in dogs, swine, and humans. In all available studies, the PDGP has been reported to be located adjacent to the PDA and to comprise on average 17 ganglia per heart in dogs, 7 in swine, and 5.2 in humans (*Table 1*).[12,24,25] Additional studies described the distribution and the amount of nerve fibres on the dorsal surface of the ventricles in different species. The systematic literature review additionally indicated that functional characterization of ventricular GPs has not been performed in detail yet, however, suggesting that they may affect both atrial and ventricular electrophysiology (*Table 2*). Taken together, current

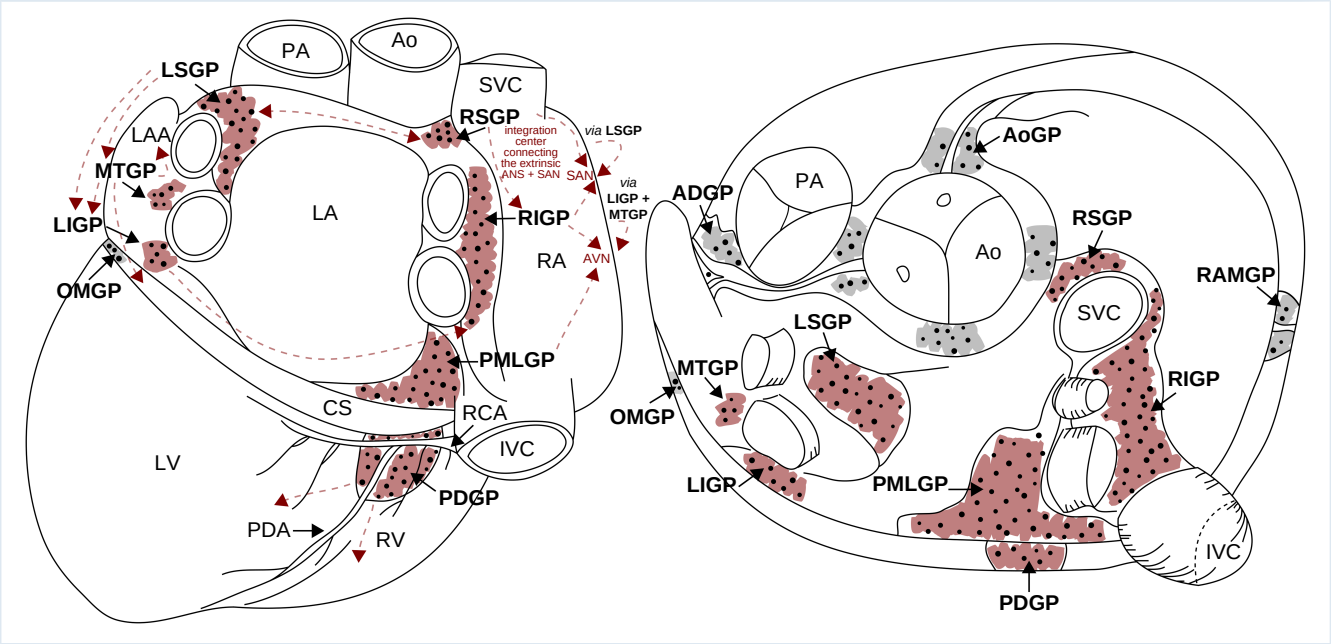

Figure 2 Schematic representation of investigated and potentially additional neuroscientific-driven clinical targets. Schematic representation of GPs with a focus on the ones that have been addressed as potential neuroscientific-driven clinical targets (red) according to current knowledge. A dorsal (left) and superior view (right) are shown. GPs that may also represent clinical targets but have not been investigated yet are additionally shown (grey). ADGP, anterior descending GP; ANS; autonomic nervous system; Ao, Aorta; AoGP, aortic root GP; AVN; atrioventricular node; CS, coronary sinus; IVC, vena cava inferior; LIGP, inferior (posterolateral) left atrial GP; LSGP, superior left atrial GP; MTGP; Marshall tract GP; PA, pulmonary artery; OMGP, obtuse marginal GP; PMLGP; posteromedial left atrial GP; PDA, posterior descending coronary artery; RA, right atrium; RAMGP, right acute marginal GP; RCA, right coronary artery; RIGP, the inferior (posterior) right atrial GP; RSGP; superior (anterior) right atrial GP; SAN; sinoatrial node; SVC, vena cava superior. Other abbreviations as in *Figure 1*. Adapted from Armour *et al.*[12]

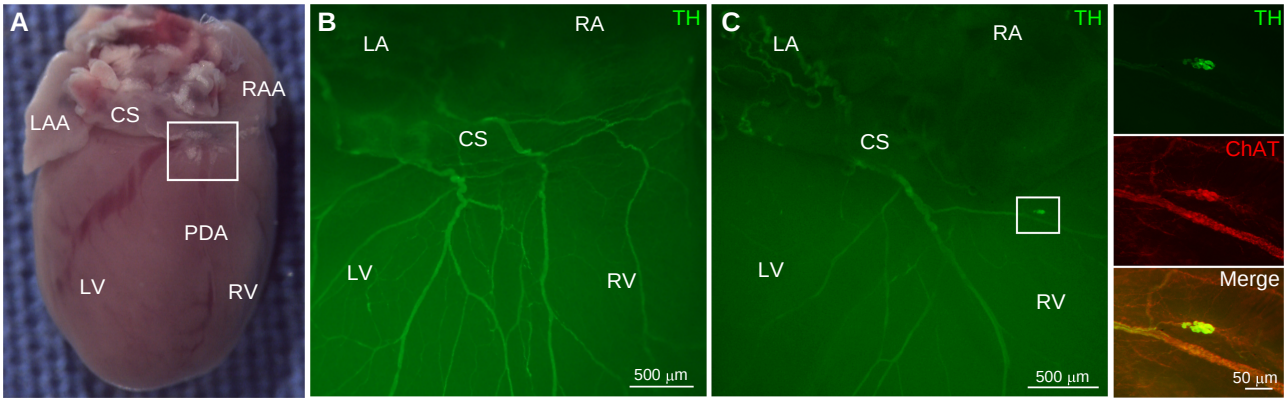

Figure 3 The neural network of the C57BL/6 murine heart. (*A*) Macrograph of the dorsal view of a murine heart visualizing the target region. (*B*, *C*) Confocal imaging of tyrosine hydroxylase (TH) and choline acetyltransferase (ChAT) illustrates nerve fibres coursing from the atria across the CS towards the apex. (*B*) Whereas in the majority of C57BL/6 murine hearts, no ventricular ganglia were present, (*C*) they were found in only selected hearts, e.g. one ganglion on the RV below the CS in one case. CS, coronary sinus; PDA, posterior descending coronary artery; RA, right atrium. Other abbreviations as in *Figure 1*.

knowledge indicates that (i) the PDGP has not been systematically studied in mice, while (ii) the PDGP morphology seems to be comparable between swine and humans considering the number of described ganglia, and (iii) functional characterization of ventricular GPs is sparse and so far, unknown for the PDGP. The PDGP as well as other GPs that have been addressed as potential neuroscientific-driven clinical targets or may represent clinical targets but have not been investigated yet are visualized in *Figure 2*.

Ventricular ganglia in mice

Whole-mount-stainings from C57BL/6 murine hearts ($n = 43$) indicated a rare presence of ventricular ganglia (10%). In animals where ventricular ganglia were found, they contained 5–8 neuronal soma located on the epicardial septum ($n = 3$) and one ganglion with 1–3 neuronal soma on the RV below the coronary sinus ($n = 1$). In all other animals, no ventricular soma were detected in the area of interest rendering C57BL/6 mice not a feasible model for detailed functional analysis (*Figure 3*). This is in line with studies from other groups, which have studied innervation of the mouse heart in the same mouse strain.[3,39,40]

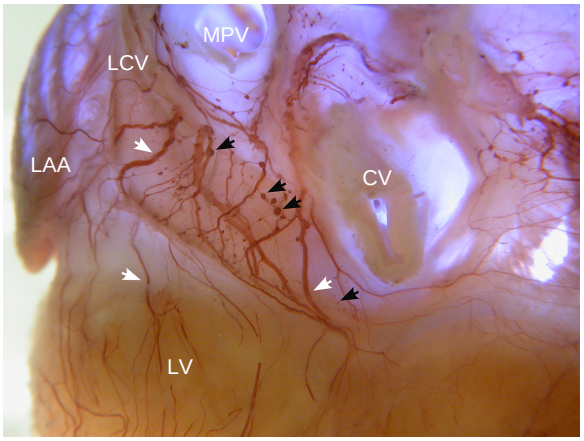

Figure 4 The epicardial neural network of the porcine heart. Macrograph of an acetylcholinesterase staining of the dorsal view of the newborn swine heart depicting the dorsal left atrial sub-plexus distributed on the root of the LCV adjacent to the PDGP with multiple epicardial ganglia (black arrowheads) from which numerous epicardial nerves (white arrowheads) extend to the posterior LV wall. CV, caudal vein; LCV, left cranial vein; MPV, middle pulmonary vein. Other abbreviations as in *Figure 1*.

Posterior descending ganglionated plexus anatomy in swine

Different from C57BL/6 mice, the presence of ventricular ganglia adjacent to epicardial adipose tissue was verified by haematoxylin–eosin (*Figure 1D*) and acetylcholinesterase (*Figure 4*) staining at the location of the PDGP in swine. This is in line with previous observations suggesting a porcine model to be reasonable for functional PDGP analysis.

Wave propagation characteristics in swine

CV during PDGP HFS (2.64 ± 0.92 m/s vs. 2.32 ± 0.49 m/s; $P = 0.477$), PDGP local nicotine (2.56 ± 0.62 m/s vs. 2.32 ± 0.49 m/s; $P = 0.571$), and systemic isoprenaline stimulation (1.93 ± 0.16 m/s vs. 2.32 ± 0.49 m/s; $P = 0.260$) did not differ compared to paced rhythm (*Figures 5A and 6*). HFS (8.52 ± 2.24 radian vs. 2.79 ± 0.89 radian; $P = 0.018$) and local nicotine stimulation (19.79 ± 6.49 radian vs. 2.79 ± 0.89 radian; $P = 0.044$) increased the dispersion of CV compared to paced rhythm, whereas systemic isoprenaline stimulation did not (2.29 ± 0.40 radian vs. 2.79 ± 0.89 radian; $P = 0.381$) (*Figures 5B* and *7*). These functional proof-of-principle studies performed in an *ex vivo* porcine model analysing a total of 4300 local unipolar electrograms from a multi-electrode sock in three hearts confirm the findings of our systematic literature review.

Activation recovery intervals in swine

During paced rhythm, ARIs did not differ between any LV and RV regions (*Figures 8A* and *9A* and *Table 3*).

Compared to paced rhythm, PDGP HFS did not have any significant effect on ARIs. However, HFS evoked regional differences resulting in an ARI prolongation in the RV. In detail, ARIs in the posterior RV (257.8 ± 6.7 ms vs. 244.8 ± 1.9 ms; $P = 0.044$) and basal RV (258.1 ± 4.2 ms vs. 244.8 ± 1.9 ms; $P = 0.039$) were longer than ARIs in the posterior LV (*Figures 8B* and *9B*).

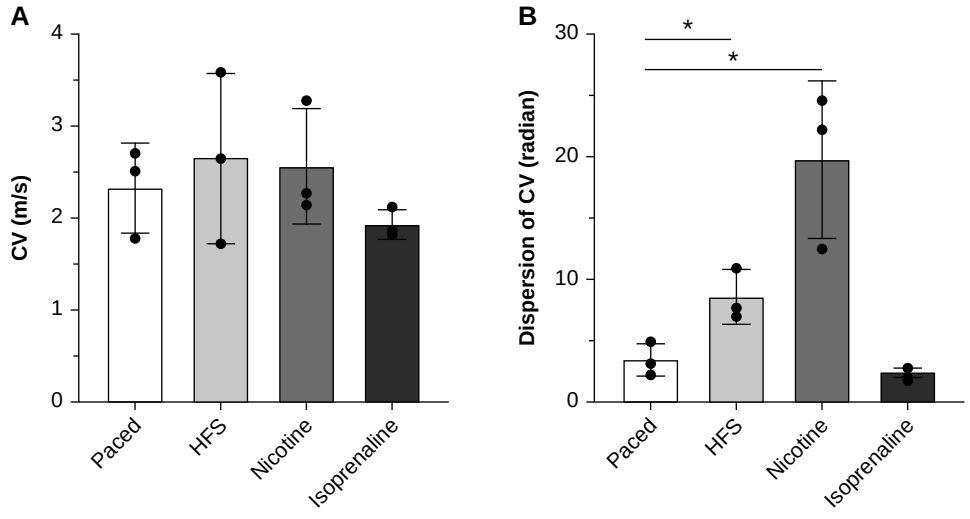

Figure 5 PDGP HFS and local nicotine stimulation increase the dispersion of CV. (*A*) CV and (*B*) dispersion of CV during paced rhythm; PDGP HFS, PDGP local nicotine and systemic isoprenaline stimulation are depicted. CV, conduction velocity; HFS, high-frequency stimulation; PDGP, posterior descending ganglionated plexus. * $P < 0.05$.

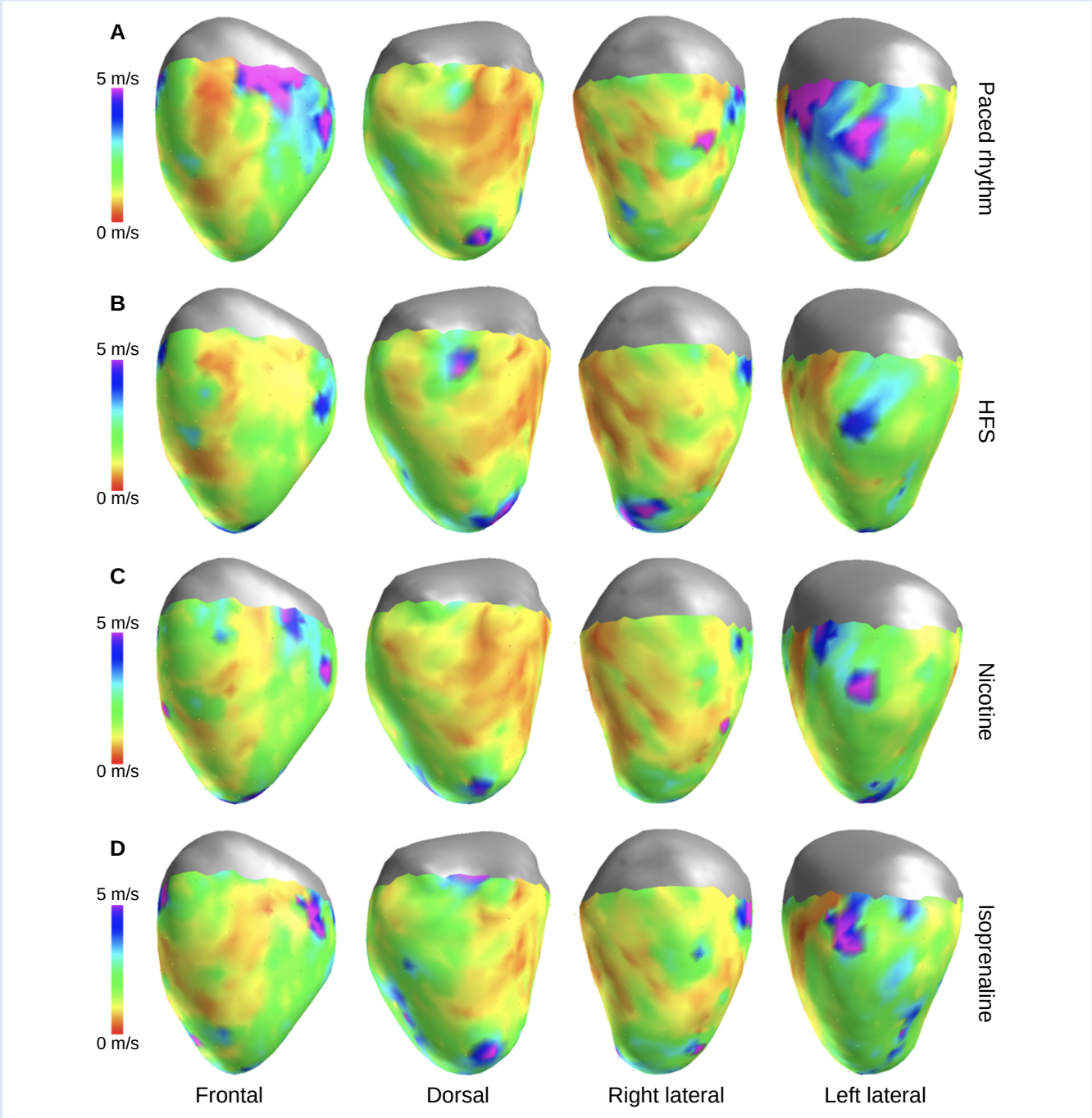

Figure 6 CV does not differ between paced rhythm and PDGP HFS, local nicotine, and systemic isoprenaline stimulation. Epicardial maps demonstrating no regional differences in CV during (*A*) paced rhythm, (*B*) PDGP HFS, (*C*) PDGP local nicotine stimulation, and (*D*) systemic isoprenaline stimulation. Abbreviations as in *Figure 4*.

During local nicotine stimulation, there were no differences between any LV and RV regions (*Figures 8C* and *9C*).

Systemic isoprenaline stimulation prolonged ARIs in the RV (276.9 ± 3.0 ms vs. 257.5 ± 4.1 ms; $P = 0.024$). Considering specific RV areas, systemic isoprenaline stimulation prolonged ARIs in the posterior (276.1 ± 7.8 ms vs. 257.3 ± 5.5 ms; $P = 0.026$), basal (275.7 ± 4.7 ms vs. 258.6 ± 2.0 ms; $P = 0.047$), and midventricular RV (278.2 ± 4.2 ms *vs.* 256.4 ± 7.1 ms; $P = 0.011$) compared to paced rhythm (*Figure 10A*). There was a trend towards longer ARIs in the anterior RV, whereas this effect was not present in the LV (*Figure 10B*). Comparing ARIs in the RV and LV during isoprenaline stimulation, ARIs in the RV were longer (276.9 ± 3.0 ms vs. 263.0 ± 3.2 ms; $P = 0.005$). In detail, ARIs in the anterior RV (275.5 ± 5.6 ms vs. 259.7 ± 3.8 ms; $P = 0.037$), posterior (276.1 ± 7.8 ms vs. 259.7 ± 3.8 ms; $P = 0.028$), basal (275.7 ± 4.7 ms vs. 259.7 ± 3.8 ms; $P = 0.034$), and midventricular RV (278.2 ± 4.2 ms vs. 259.7 ± 3.8 ms; $P = 0.012$) were longer than in the posterior LV. Similarly, ARIs in the anterior RV (275.5 ± 5.6 ms vs. 259.2 ± 3.7 ms; $P = 0.030$), posterior

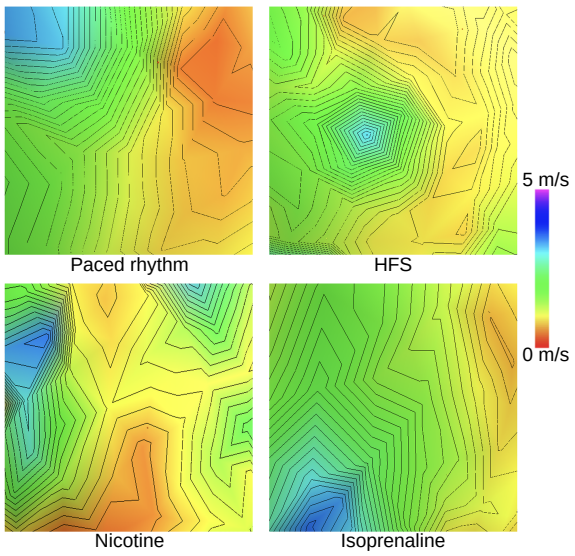

Figure 7 PDGP HFS and local nicotine stimulation increase the dispersion of CV. Representative colour-coded isochronal reconstructions are illustrated. PDGP HFS and local nicotine stimulation increased the dispersion of CV compared to paced rhythm. Abbreviations as in *Figure 5*.

(276.1 ± 7.8 ms vs. 259.2 ± 3.7 ms; $P = 0.023$), basal (275.7 ± 4.7 ms vs. 259.2 ± 3.7 ms; $P = 0.028$), and midventricular RV (278.2 ± 4.2 ms vs. 259.2 ± 3.7 ms; $P = 0.009$) were longer than in the basal LV (*Figures 8D, 9D, and 10D*). ARI values during paced rhythm, PDGP HFS, local nicotine, and systemic isoprenaline are additionally visualized in a heatmap (*Figure 11*).

There were no differences in electrogram amplitude during paced rhythm, PDGP HFS, local nicotine, and systemic isoprenaline stimulation (1.24 ± 0.77 mV vs. 1.28 ± 0.83 mV vs. 1.31 ± 0.87 mV vs. 1.28 ± 0.83 mV; $P = 0.595$) as supported by a performed sub-group analysis of 2000 local electrograms. Electrogram morphology was not altered during PDGP stimulation (*Figure 10C*).

Posterior descending ganglionated plexus anatomy in humans

Morphological analysis of explanted human hearts suggested a close anatomical relationship of the PDGP, located at the septum near the ostium of the coronary sinus, and the origin of the PDA as well as the posteromedial left atrial GP, which is located in close proximity (*Figure 12*). Localization of the PDGP was aggravated by the presence of epicardial adipose tissue on top of the PDA.

Analysis of three-dimensionally reconstructed hearts suggested the localization of the PDGP in all cases. The PDGP was illustrated at the coronary sinus within epicardial adipose tissue with ~3 mm towards the posteromedial left atrial GP (*Figure 13*). The PDGP was characterized by inter-patient anatomical variability with a mean size of 20.0 ± 2.4 cm^2 ranging from 9.5 to 33.4 cm^2 (*Figure 14*). There was no

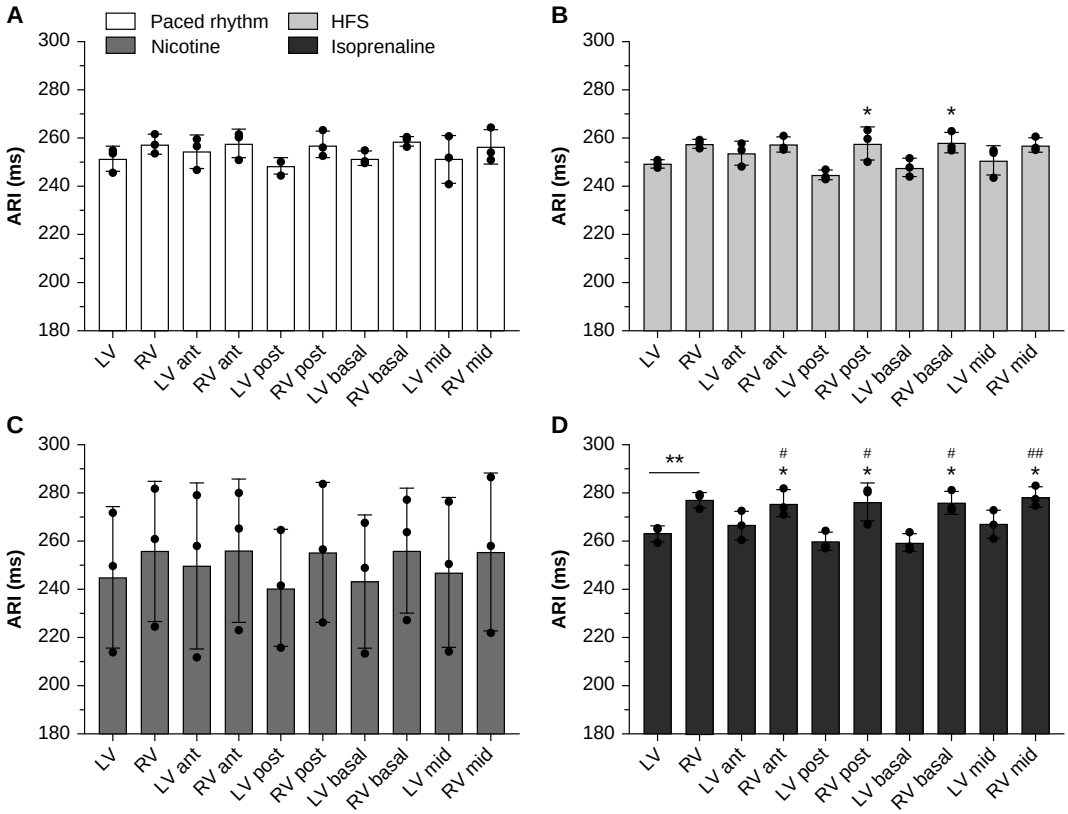

Figure 8 PDGP HFS and systemic isoprenaline stimulation evoke regional differences in ARIs. Regional ARIs during (*A*) paced rhythm, (*B*) PDGP HFS, (*C*) PDGP local nicotine stimulation, and (*D*) systemic isoprenaline stimulation are illustrated. ARIs in all LV and RV areas were compared with each other, with significant results visualized here. Abbreviations as in *Figures 1* and *5*. *Compared to LV post, # compared to LV basal, */# $P < 0.05$, **/## $P < 0.01$.

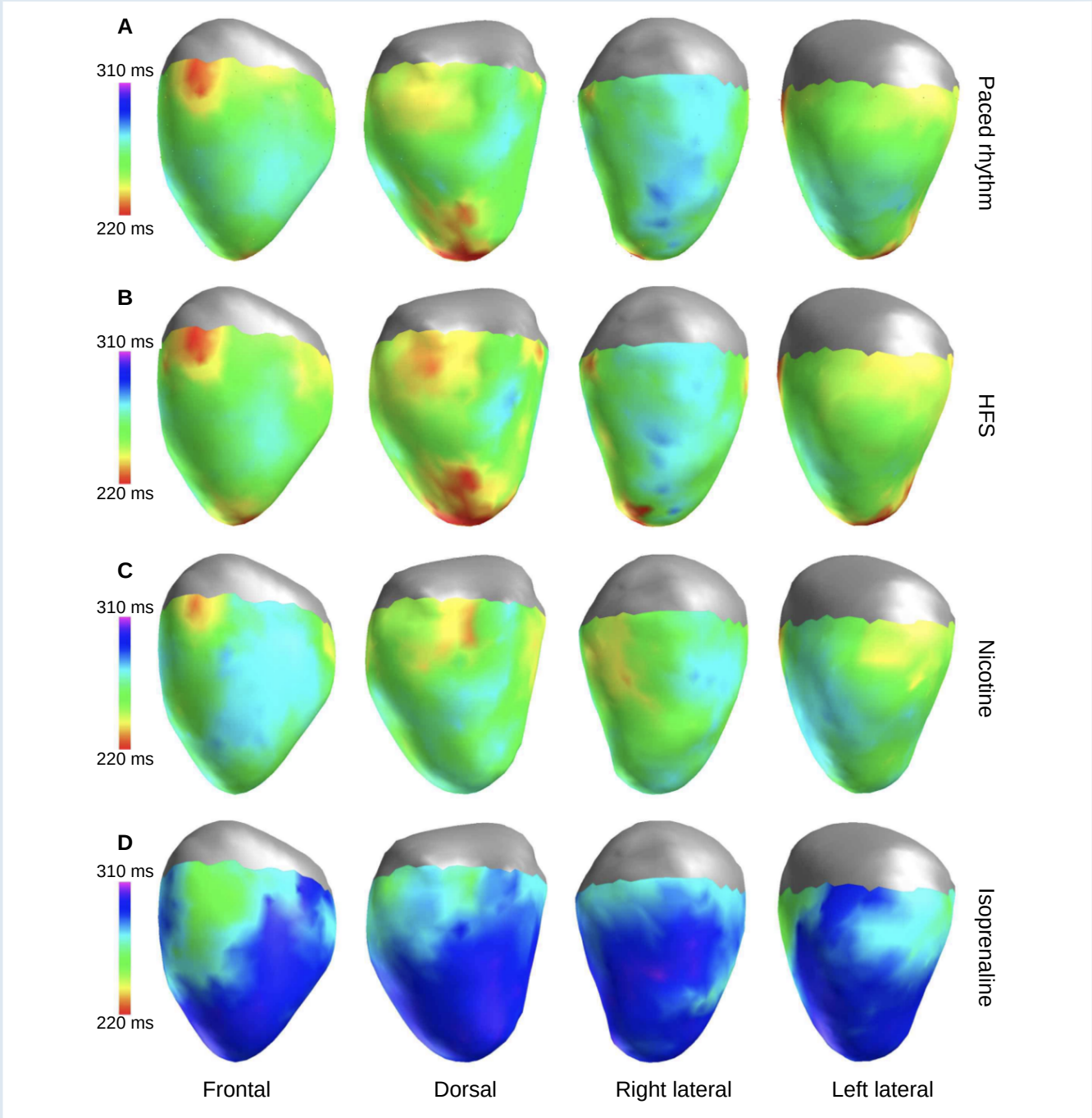

Figure 9 PDGP HFS and systemic isoprenaline stimulation prolong ARIs in the RV. Representative epicardial maps of ARIs during (*A*) paced rhythm, (*B*) PDGP HFS, (*C*) PDGP local nicotine stimulation, and (*D*) systemic isoprenaline stimulation are depicted. Abbreviations as in *Figures 1* and *5*.

difference in the suggested PDGP size between patients with ventricular arrhythmia and underlying structural heart diseases vs. patients with atrial fibrillation/atrial tachycardia without any structural heart disease (21.9 ± 4.4 cm^2 vs. 18.2 ± 1.8 cm^2; $P = 0.523$).

Discussion

The present proof-of-principle study investigated the role of the PDGP for neural control of cardiac electrophysiology in different species characterizing ventricular innervation in a translational approach. The main findings are that (i) species-dependent differences considering the presence of the PDGP exist, (ii) ventricular GPs are rarely present in C57BL/6 murine hearts, (iii) in an *ex vivo* porcine model, PDGP HFS and local nicotine stimulation increase the dispersion of CV, (iv) PDGP HFS evokes regional differences in ARIs, and (v) the PDGP is regularly present in human hearts located near the PDA and the posteromedial left atrial GP within epicardial adipose tissue and its localization can be suggested using three-dimensional reconstructions of the human heart illustrating inter-patient anatomical variability.

Table 3 Activation recovery intervals in swine

	LV	RV
Paced rhythm		
Total	251.4 ± 5.1	257.5 ± 4.1
Anterior	254.4 ± 6.8	257.7 ± 5.9
Posterior	248.4 ± 3.3	257.3 ± 5.5
Basal	251.7 ± 3.0	258.6 ± 2.0
Mid	251.2 ± 9.9	256.4 ± 7.1
HFS		
Total	249.3 ± 2.0	258.3 ± 2.1
Anterior	253.2 ± 6.2	257.4 ± 3.2
Posterior	244.8 ± 1.9	257.8 ± 6.7
Basal	248.6 ± 3.7	258.1 ± 4.2
Mid	252.3 ± 4.3	257.2 ± 3.1
Nicotine		
Total	245.0 ± 29.3	255.7 ± 29.0
Anterior	249.5 ± 34.5	256.0 ± 29.5
Posterior	240.5 ± 24.3	255.3 ± 28.8
Basal	243.2 ± 27.5	256.0 ± 25.7
Mid	246.8 ± 31.0	255.4 ± 32.5
Isoprenaline		
Total	263.0 ± 3.2	276.9 ± 3.0
Anterior	267.2 ± 5.2	275.5 ± 5.6
Posterior	259.7 ± 3.8	276.1 ± 7.8
Basal	259.2 ± 3.7	275.7 ± 4.7
Mid	267.4 ± 5.0	278.2 ± 4.2

HFS, high-frequency stimulation; LV, left ventricle; RV, right ventricle.

Role of ventricular ganglionated plexus

During the last decades, cardiac innervation has been studied in various species[41] with generally accepted inter-individual and species-dependent differences.[2,12] These results are supplemented by the here presented inter-individual variability considering detected ventricular ganglia in C57BL/6 mice, and the consistent finding of the PDGP in swine. Even though initially human ventricles have been reported to contain only a minority of ganglia, Armour *et al.* delineated relatively large populations identifying five ventricular GPs: (i) the major ventricular GP (aortic root GP), embedded in fat surrounding the aortic root, and adjacent to their eponymous coronary arteries, (ii) the anterior descending GP, (iii) the right acute marginal GP, (iv) the obtuse marginal GP, and (v) the PDGP.[12] During further in-depth studies in the human heart, Pauza *et al.* described a system of seven sub-plexus[2] thereby laying the cornerstone for subsequent functional analyses and improving the understanding of the structural organization of the intrinsic cardiac nervous system.[35,36,42]

Following the initial assumption that ventricular electrophysiology is mainly controlled by post-ganglionic sympathetic efferent axons,[43] ventricular innervation by parasympathetic fibres and changes in ventricular repolarization after cervical vagal nerve stimulation have been reported.[44] Meanwhile, studies in various species revealed that ventricular GPs possess both adrenergic and cholinergic neurons as well as inter-neurons.[41,42] Our proof-of-principle observations from an *ex vivo* porcine model now extend these results indicating global and regional changes in ventricular electrophysiological control including the dispersion of CV in response to local PDGP stimulation.

For more than two decades, dispersion of CV has been known to be a more important determinant of myocardial vulnerability to ventricular fibrillation than dispersion in refractoriness, suggesting its contribution to the proarrhythmic effects of acute myocardial ischaemia.[45] In line with this, its incremental value has recently been underlined by the observation that increased dispersion of CV is a stronger predictor of critical ventricular tachycardia sites than homogeneously slow CV or increased ARI dispersion.[46] Ventricular ganglia have further been demonstrated to undergo morphological and phenotypic remodelling after myocardial infarction. Whereas afferent neural signals from the infarcted region to intrinsic cardiac neurons are attenuated, those from border and remote regions are preserved, creating a 'neural sensory border zone'.[47] Our now presented results from healthy swine hearts indicate that the PDGP contributes to ventricular electrophysiological control. Increased dispersion of CV potentially serves as a determinant of electrical heterogeneity, which might provoke the occurrence of arrhythmias. However, we cannot exclude the possibility that transmural conduction and wave breakthroughs might have affected CV measurements.

Nicotinic stimulation of individual GPs in dogs has been revealed to result in distinct regional patterns of repolarization, with both atrial and ventricular GPs, the latter including the right ventricular, ventral septal ventricular, and cranial medial ventricular GP, affecting ventricular repolarization properties.[37] Our finding of an increased global dispersion of CV following local PDGP nicotine stimulation is in line with this concept of a widespread impact of individual GPs. Since neurons in each major GP have been shown to be in constant communication with one another,[12] we do not know whether this is a direct or indirect effect mediated via other GPs. Still, the nicotine effect observed in our study may be variable depending on the species as well as the injection site and dose.

Isoprenaline has been shown to result in either a prolongation or a shortening of action potential duration with species-dependent differences.[48] This is confirmed by the here observed ARI prolongation in the RV compared to paced rhythm, corroborating prior findings in swine.[49] Importantly, regional differences in ARIs during systemic isoprenaline stimulation represent an adequate response to catecholamines validating the operability of the presented *ex vivo* model. Further functional analysis of ventricular GPs is necessary, as e.g. modification of the major aortic root GP with low-level electrical stimulation has been reported to result in suppression of atrial fibrillation inducibility,[38] but its effect on ventricular electrophysiological control has not been completely understood.

Potential clinical implications

Based on sparse functional characterization of ventricular innervation, potential clinical implications of modulation of individual ventricular GPs can only be hypothesized in health and disease despite anatomical and neurophysiological similarities of the intrinsic cardiac nervous system in the porcine and the human heart.[12,24] Previous observations suggested an impact of atrial GPs on ventricular electrophysiology,[37] as low-intensity atrial GP stimulation has been shown to protect against ventricular arrhythmias during acute myocardial infarction in a canine model.[50] However, despite the existing impact of inter-connecting GPs on atrial and ventricular electrophysiology, ventricular GP stimulation has been demonstrated to result in a higher incidence of widespread biventricular repolarization changes compared to atrial GP stimulation.[37] These prior results underline the importance of the here suggested clinical implications of functional PDGP characterization including improved understanding of ventricular arrhythmogenesis and the potential as well as limitations of targeted neuromodulation techniques. Considering the anatomical proximity of the PDGP and the PDA,

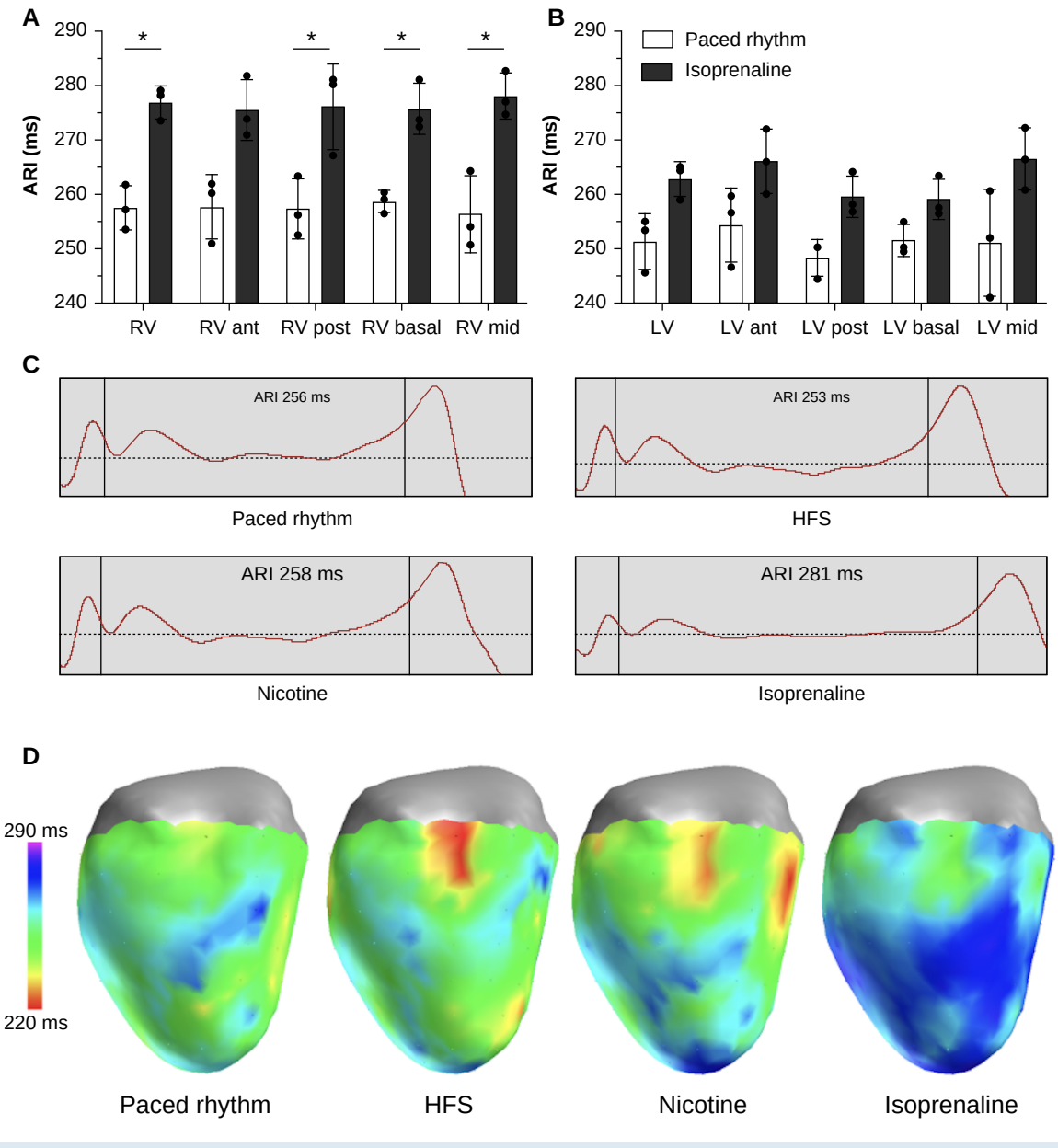

Figure 10 Systemic isoprenaline stimulation prolongs ARIs in the RV compared to paced rhythm. Regional ARIs in the (*A*) RV and (*B*) LV during paced rhythm and systemic isoprenaline stimulation are depicted. (*C*) One exemplary unipolar signal from a single sock electrode demonstrates ARI determination without any alterations in unipolar electrogram morphology. (*D*) Epicardial ARI maps from a dorsal projection show ARI prolongation during systemic isoprenaline stimulation. Abbreviations as in *Figures 1* and *5*. *$P < 0.05$.

one might speculate that acute and chronic changes in autonomic function might be related to cardiac arrhythmogenesis. This might be of specific relevance, e.g. during acute reperfusion-mediated and chronic post-myocardial infarction arrhythmias. Therefore, investigation of (i) ventricular GP function with assessment of GP inter-actions and (ii) the feasibility of radiofrequency catheter-based ventricular GP modulation via adjacent coronary arteries or epicardial approaches may help to develop potential therapeutic antiarrhythmic approaches. Consequently, the here presented results will hopefully pave the way for future studies including humans for a deepened physiological understanding in health and disease including neural control during myocardial infarction and remodelling thereafter with respect to ventricular arrhythmogenesis. As this proof-of-principle study was of explorative nature, performance of a catheter-based ablation approach and comparison to ablation of atrial GPs was beyond the scope of the presented set-up of experiments.

Furthermore, the PDGP is located at the septum close to the posteromedial left atrial GP, which is the final common pathway of the left vagus innervating the atrioventricular node and increasingly targeted in recent times during cardioneuroablation procedures.[19–21] Detailed variants and comparison within and between species regarding the localization with respect to the posterior coronary groove have been described previously.[6] One might speculate that in case of widespread ablation in these patients with reflex syncope, extents of the PDGP

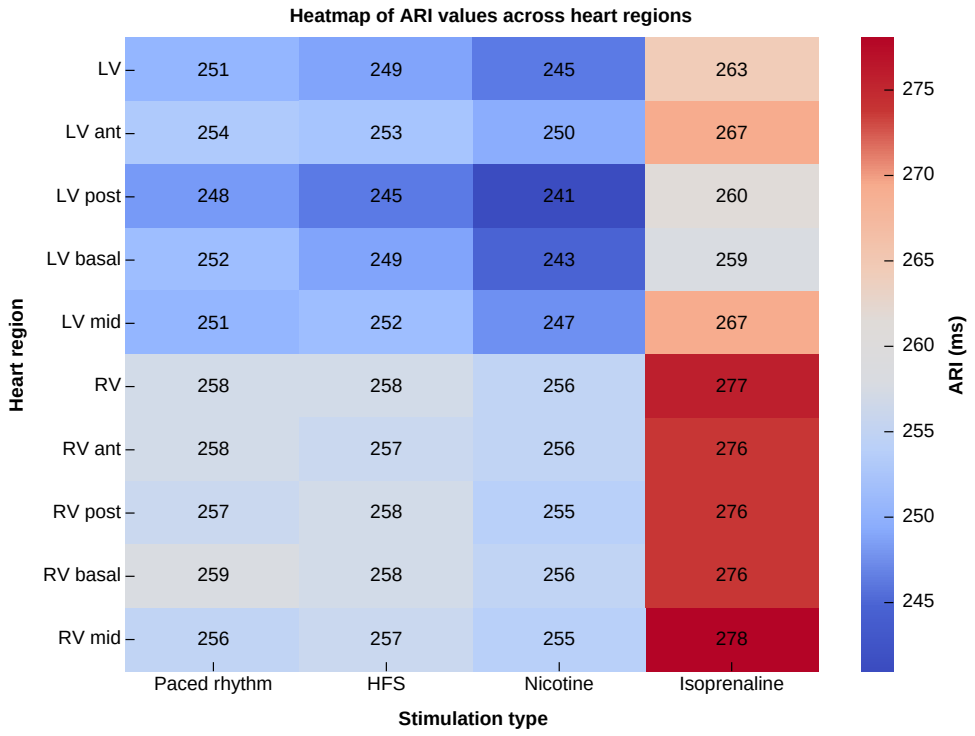

Figure 11 Heatmap of ARI values across different heart regions. Heatmap visualizing ARI values during paced rhythm, PDGP HFS, PDGP local nicotine stimulation, and systemic isoprenaline stimulation. Abbreviations as in *Figures 1* and *5*.

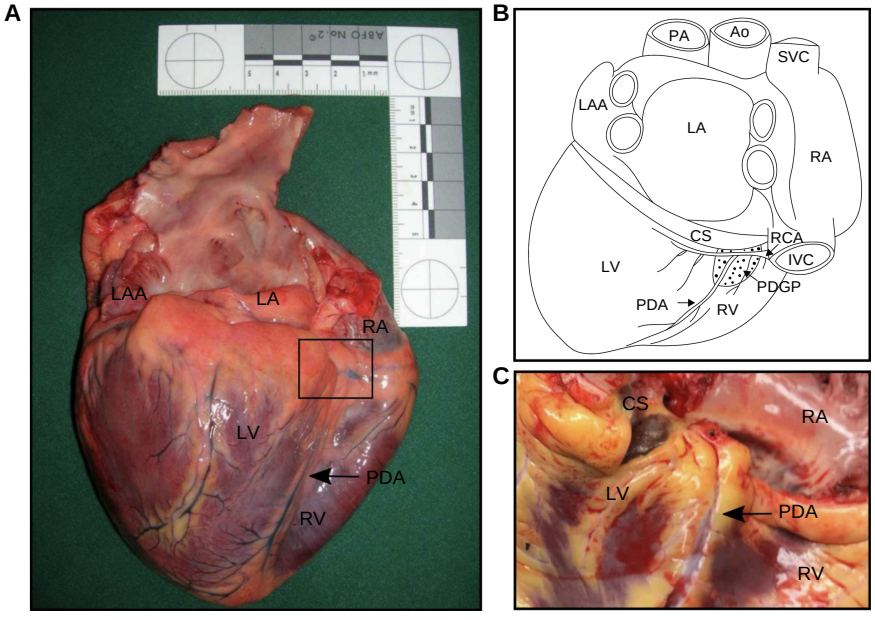

Figure 12 Potential challenges regarding translational outlook. Macrographs of the dorsal view of (*A*) a human heart, (*B*) a schematic drawing, and (*C*) a detailed view of a human heart visualizing the location of the PDGP. (*A*) The area of the PDGP disappearing within the Sulcus interventricularis posterior is marked. (*B*) The PDGP is located at the septum close to the CS ostium and the posteromedial left atrial GP. The close anatomical relationship of the PDGP and the PDA origin is demonstrated. (*C*) Determination of the PDGP localization associated with the PDA is aggravated by distinct adjacent epicardial adipose tissue. Ao, Aorta; CS, coronary sinus; IVC, vena cava inferior; PA, pulmonary artery; PDA, posterior descending coronary artery; RA, right atrium; RCA, right coronary artery; SVC, vena cava superior. Other abbreviations as in *Figure 1*. Adapted from Armour *et al.*[12]

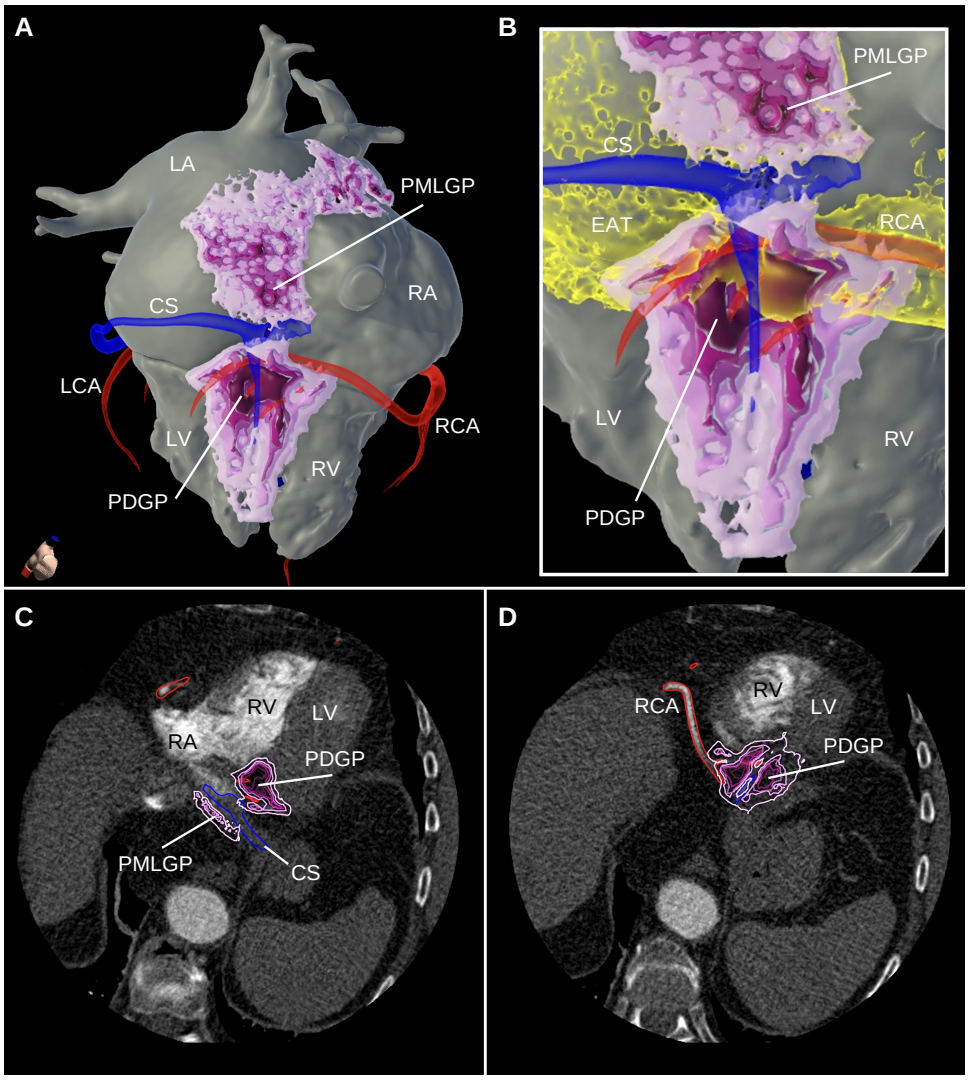

Figure 13 Three-dimensional reconstruction of the PDGP area in the human heart. (*A*) Three-dimensional reconstruction suggests the localization of the PDGP at the septum close to the CS ostium, the RCA and the PMLGP. (*B*) Detailed view of the suggested PDGP localization demonstrates adjacent EAT as well as the close relationship to the PMLGP. Computed tomography axial scans visualize the suggested localization at the septum close to the (*C*), CS and PMLGP and (*D*), the RCA. LCA, left coronary artery; PMLGP; posteromedial left atrial GP; RA, right atrium. Other abbreviations as in *Figures 1* and *11*.

could be targeted, thus, affecting ventricular electrophysiology. To date, the impact of potentially related effects during the long run, e.g. after myocardial infarction or the development of diabetic autonomic neuropathy is not known.[21] In this context, pre-/intra-procedural imaging may help to provide anatomy and substrate characterization and therefore guidance to avoid unintended neuromodulation. Consequently, the here presented translational approach to ventricular innervation suggests that the localization and the role of the PDGP for neural control of cardiac electrophysiology are important to consider for improved cardioneuroablation procedures in the future.

Study limitations

This proof-of-principle study in structurally healthy hearts has some limitations. First, murine studies were performed in C57BL/6 hearts only. Whereas, C57BL/6 mice do not appear to be a feasible model for detailed functional analysis, which is in line with previous studies in the same mouse strain,[3,39,40] other murine backgrounds might be different. Second, the here described observations of ventricular electrophysiological control during PDGP modification in an *ex vivo* model with disrupted central inputs may differ from *in vivo* conditions. Third, considering possible inter-individual anatomic variations, PDGP HFS and local nicotine stimulation may not have elicited the same effect in all animals. Still, in order to avoid a failure in response, nicotine was broadly injected into the region of the PDGP in our porcine model, in line with well-established protocols.[37] The PDGP was identified at the cranial aspect of the dorsal interventricular groove, located surrounding the first centimetre of its eponymous coronary artery. Fourth, the ventricular effective refractory period was not measured in this study. Whereas, the ARI is used as a surrogate for local action potential duration and an accepted method in experimental electrophysiology, correlation with the ventricular effective refractory period would provide

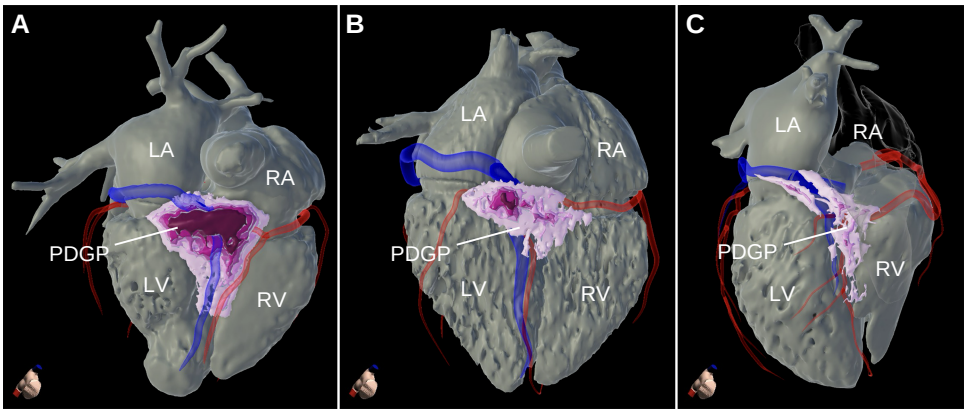

Figure 14 Inter-patient anatomical variability of the PDGP area in three-dimensionally reconstructed human hearts. Inter-patient anatomical variability of the suggested PDGP area is illustrated. These originate from (*A*), a patient with ischaemic cardiomyopathy and ventricular tachycardia, (*B*), a patient with dilated cardiomyopathy and pre-mature ventricular contractions and (*C*), a patient with perimyocarditis and pre-mature ventricular contractions. RA, right atrium. Other abbreviations as in *Figure 1*.

physiological validation of this surrogate in the *ex vivo* porcine model. Future studies should consider incorporating direct measures of refractoriness to complement ARI data. Fifth, the here presented study has a small sample size. As this proof-of-principle study was of explorative nature, sample size calculation was chosen based on previous studies in large animals and literature review according to current state-of-the-art experimental set-up and practicability to assess optimal conditions for the here presented proof-of-principle study.[9,10] Accurate prediction of the effect size regarding the impact of the PDGP on neural control of cardiac electrophysiology might differ within and between species.

Conclusions

The present translational approach to ventricular innervation demonstrates first evidence of the functional relevance of the PDGP located within epicardial adipose tissue, with morphological findings indicating important species-related differences with potentially several anatomical variations. These may contribute to the understanding of neurally mediated ventricular arrhythmias. The close proximity to the posteromedial left atrial GP in humans should be considered during cardioneuroablation procedures.

Acknowledgements

The authors kindly thank P. Lietz for his technical support with *ex vivo* experiments in swine, J. P. Sperhake for providing the photograph of a human heart, and the Department of Oral and Maxillofacial Surgery, University Medical Center Hamburg–Eppendorf for providing animals for the *ex vivo* porcine model. Part of the Central Illustration was created with BioRender.com.

Funding

This work was supported by the DZHK (German Centre for Cardiovascular Research), Berlin, Germany (FKZ 81Z0710112 to C.M.), a Leducq International Network of Excellence Award (23CVD04) on Bioelectronics for Neurocardiology (to C.M.) and Interreg (Beat the Rhythm 33142 to A.-K.K., K.S., and C.M.).

Conflict of interest: none declared.

Data availability

The data underlying this article will be shared on reasonable request to the corresponding author.

References

1. Mills TW. Rhythm and innervation of the heart of the sea-turtle. *J Anat Physiol* 1886;**21**:1–20.1.
2. Pauza DH, Skripka V, Pauziene N, Stropus R. Morphology, distribution, and variability of the epicardiac neural ganglionated subplexuses in the human heart. *Anat Rec* 2000;**259**:353–82.
3. Rysevaite K, Saburkina I, Pauziene N, Vaitkevicius R, Noujaim SF, Jalife J *et al.* Immunohistochemical characterization of the intrinsic cardiac neural plexus in whole-mount mouse heart preparations. *Heart Rhythm* 2011;**8**:731–8.
4. Janes RD, Christopher Brandys J, Hopkins DA, Johnstone DE, Murphy DA, Armour JA. Anatomy of human extrinsic cardiac nerves and ganglia. *Am J Cardiol* 1986;**57**:299–309.
5. Hanna P, Buch E, Stavrakis S, Meyer C, Tompkins JD, Ardell JL *et al.* Neuroscientific therapies for atrial fibrillation. *Cardiovasc Res* 2021;**117**:1732–45.
6. Aksu T, Gopinathannair R, Gupta D, Pauza DH. Intrinsic cardiac autonomic nervous system: what do clinical electrophysiologists need to know about the "heart brain"? *J Cardiovasc Electrophysiol* 2021;**32**:1737–47.
7. Crick SJ, Anderson RH, Yen SH, Sheppard MN. Localisation and quantitation of autonomic innervation in the porcine heart II: endocardium, myocardium and epicardium. *J Anat* 1999;**195(Pt 3)**:359–73.
8. Kim MY, Nesbitt J, Koutsoftidis S, Brook J, Pitcher DS, Cantwell CD *et al.* Immunohistochemical characteristics of local sites that trigger atrial arrhythmias in response to high-frequency stimulation. *Europace* 2023;**25**:726–38.
9. Kahle AK, Klatt N, Jungen C, Dietenberger A, Kuklik P, Münkler P *et al.* Acute modulation of left ventricular control by selective intracardiac sympathetic denervation. *J Am Coll Cardiol EP* 2023;**9**:371–84.
10. Meyer C, Rana OR, Saygili E, Gemein C, Becker M, Nolte KW *et al.* Augmentation of left ventricular contractility by cardiac sympathetic neural stimulation. *Circulation* 2010;**121**:1286–94.
11. Saburkina I, Rysevaite K, Pauziene N, Mischke K, Schauerte P, Jalife J *et al.* Epicardial neural ganglionated plexus of ovine heart: anatomic basis for experimental cardiac electrophysiology and nerve protective cardiac surgery. *Heart Rhythm* 2010;**7**:942–50.
12. Armour JA, Murphy DA, Yuan BX, Macdonald S, Hopkins DA. Gross and microscopic anatomy of the human intrinsic cardiac nervous system. *Anat Rec* 1997;**247**:289–98.
13. Stavrakis S, Nakagawa H, Po SS, Scherlag BJ, Lazzara R, Jackman WM. The role of the autonomic ganglia in atrial fibrillation. *J Am Coll Cardiol EP* 2015;**1**:1–13.
14. Hou Y, Scherlag BJ, Lin J, Zhang Y, Lu Z, Truong K *et al.* Ganglionated plexi modulate extrinsic cardiac autonomic nerve input. Effects on Sinus rate, atrioventricular conduction, refractoriness, and inducibility of atrial fibrillation. *J Am Coll Cardiol* 2007;**50**:61–8.
15. Eickholt C, Jungen C, Drexel T, Alken F, Kuklik P, Muehlsteff J *et al.* Sympathetic and parasympathetic coactivation induces perturbed heart rate dynamics in patients with paroxysmal atrial fibrillation. *Med Sci Monit* 2018;**24**:2164–72.

16. Pappone C, Santinelli V, Manguso F, Vicedomini G, Gugliotta F, Augello G *et al.* Pulmonary vein denervation enhances long-term benefit after circumferential ablation for paroxysmal atrial fibrillation. *Circulation* 2004;**109**:327–34.
17. Scherschel K, Hedenus K, Jungen C, Lemoine MD, Rübsamen N, Veldkamp MW *et al.* Cardiac glial cells release neurotrophic S100B upon catheter-based treatment of atrial fibrillation. *Sci Transl Med* 2019;**11**:eaav7770.
18. Scherschel K, Hedenus K, Jungen C, Münkler P, Willems S, Anwar O *et al.* Impact of the ablation technique on release of the neuronal injury marker S100B during pulmonary vein isolation. *Europace* 2020;**22**:1502–8.
19. Pachon JC, Pachon EI, Pachon JC, Lobo TJ, Pachon MZ, Vargas RNA *et al.* Cardioneuroablation'—new treatment for neurocardiogenic syncope, functional AV block and sinus dysfunction using catheter RF-ablation. *Europace* 2005;**7**:1–13.
20. Brignole M, Aksu T, Calò L, Debruyne P, Deharo JC, Fanciulli A *et al.* Clinical controversy: methodology and indications of cardioneuroablation for reflex syncope. *Europace* 2023;**25**:euad033.
21. Aksu T, Brignole M, Calo L, Debruyne P, Di Biase L, Deharo JC *et al.* Cardioneuroablation for the treatment of reflex syncope and functional bradyarrhythmias: a scientific statement of the European Heart Rhythm Association (EHRA) of the ESC, the Heart Rhythm Society (HRS), the Asia Pacific Heart Rhythm Society (APHRS) and the Latin American Heart Rhythm Society (LAHRS). *Europace* 2024;**26**:euae206.
22. Pauziene N, Rysevaite-Kyguoliene K, Alaburda P, Pauza AG, Skukauskaite M, Masaityte A *et al.* Neuroanatomy of the pig cardiac ventricles. A stereomicroscopic, confocal and electron microscope study. *Anat Rec* 2017;**300**:1756–80.
23. Saburkina I, Pauziene N, Solomon OI, Rysevaite-Kyguoliene K, Pauza DH. Comparative gross anatomy of epicardiac ganglionated nerve plexi on the human and sheep cardiac ventricles. *Anat Rec* 2023;**306**:2302–12.
24. Arora RC, Waldmann M, Hopkins DA, Armour JA. Porcine intrinsic cardiac ganglia. *Anat Rec* 2003;**271A**:249–58.
25. Yuan BX, Ardell JL, Hopkins DA, Losier AM, Armour JA. Gross and microscopic anatomy of the canine intrinsic cardiac nervous system. *Anat Rec* 1994;**239**:75–87.
26. Jungen C, Scherschel K, Eickholt C, Kuklik P, Klatt N, Bork N *et al.* Disruption of cardiac cholinergic neurons enhances susceptibility to ventricular arrhythmias. *Nat Commun* 2017;**8**:14155.
27. Jungen C, Scherschel K, Bork NI, Kuklik P, Eickholt C, Kniep H *et al.* Impact of intracardiac neurons on cardiac electrophysiology and arrhythmogenesis in an ex vivo Langendorff system. *J Vis Exp* 2018;**22**:57617.
28. Klatt N, Scherschel K, Schad C, Lau D, Reitmeier A, Kuklik P *et al.* Development of non-fibrotic left ventricular hypertrophy in an ANG II-induced chronic ovine hypertension model. *Physiol Rep* 2016;**4**:e12897.
29. Pauza DH, Rysevaite-Kyguoliene K, Vismantaite J, Brack KE, Inokaitis H, Pauza AG *et al.* A combined acetylcholinesterase and immunohistochemical method for precise anatomical analysis of intrinsic cardiac neural structures. *Ann Anat* 2014;**196**:430–40.
30. Jazayeri MR, Vanwyhe G, Avitall B, McKinnie J, Tchou P, Akhtar M. Isoproterenol reversal of antiarrhythmic effects in patients with inducible sustained ventricular tachyarrhythmias. *J Am Coll Cardiol* 1989;**14**:705–11.
31. Friedrichs K, Adam M, Remane L, Mollenhauer M, Rudolph V, Rudolph TK *et al.* Induction of atrial fibrillation by neutrophils critically depends on CD11b/CD18 integrins. *PLoS One* 2014;**9**:e89307.
32. Münkler P, Klatt N, Scherschel K, Kuklik P, Jungen C, Cavus E *et al.* Repolarization indicates electrical instability in ventricular arrhythmia originating from papillary muscle. *Europace* 2023;**25**:688–97.
33. Benabou L, Ciro A, Soré B, Cherbi M, Labrousse R, Tixier R, *et al.* A CT-based evaluation and comparison of ganglionated plexus targeting techniques for cardioneuroablation. *Heart Rhythm* 2025:S1547-5271(25)00027-X. doi:10.1016/j.hrthm.2025.01.013
34. Jungen C, Scherschel K, Flenner F, Jee H, Rajendran P, De Jong KA, *et al.* Increased arrhythmia susceptibility in type 2 diabetic mice related to dysregulation of ventricular sympathetic innervation. *Am J Physiol Heart Circ Physiol.* 2019;**317**:H1328–41.
35. Tanaka A, Tanaka S, Miyamoto K, Yi SQ, Nakatani T. Gross anatomical study of the sympathetic cardiac nerves in the house musk shrew (Suncus murinus). *Anat Rec* 2007;**290**:468–76.
36. Rysevaite K, Saburkina I, Pauziene N, Noujaim SF, Jalife J, Pauza DH. Morphologic pattern of the intrinsic ganglionated nerve plexus in mouse heart. *Heart Rhythm* 2011;**8**:448–54.
37. Cardinal R, Pagé P, Vermeulen M, Ardell JL, Armour JA. Spatially divergent cardiac responses to nicotinic stimulation of ganglionated plexus neurons in the canine heart. *Auton Neurosci* 2009;**145**:55–62.
38. Wang HT, Xu M, Fan B, Liu XT, Su FF, Zeng D *et al.* Low-level electrical stimulation of aortic root ventricular ganglionated plexi attenuates autonomic nervous system-mediated atrial fibrillation. *J Am Coll Cardiol EP* 2015;**1**:390–7.
39. Pauza DH, Rysevaite K, Inokaitis H, Jokubauskas M, Pauza AG, Brack KE *et al.* Innervation of sinoatrial nodal cardiomyocytes in mouse. A combined approach using immunofluorescent and electron microscopy. *J Mol Cell Cardiol* 2014;**75**:188–97.
40. Pauza DH, Saburkina I, Rysevaite K, Inokaitis H, Jokubauskas M, Jalife J *et al.* Neuroanatomy of the murine cardiac conduction system. A combined stereomicroscopic and fluorescence immunohistochemical study. *Auton Neurosci* 2013;**176**:32–47.
41. Wink J, van Delft R, Notenboom RGE, Wouters PF, DeRuiter MC, Plevier JWM *et al.* Human adult cardiac autonomic innervation: controversies in anatomical knowledge and relevance for cardiac neuromodulation. *Auton Neurosci* 2020;**227**:102674.
42. Petraitiene V, Pauza DH, Benetis R. Distribution of adrenergic and cholinergic nerve fibres within intrinsic nerves at the level of the human heart hilum. *Eur J Cardiothorac Surg* 2014;**45**:1097–105.
43. Brack KE, Coote JH, Ng GA. The effect of direct autonomic nerve stimulation on left ventricular force in the isolated innervated Langendorff perfused rabbit heart. *Auton Neurosci* 2006;**124**:69–80.
44. Yamakawa K, So EL, Rajendran PS, Hoang JD, Makkar N, Mahajan A *et al.* Electrophysiological effects of right and left vagal nerve stimulation on the ventricular myocardium. *Am J Physiol Heart Circ Physiol* 2014;**307**:H722–31.
45. Sims JJ, Miller AW, Ujhelyi MR, Sims J. Electrical heterogeneity and arrhythmogenesis: importance of conduction velocity dispersion. *J Cardiovasc Pharmacol* 2003;**41**:795–803.
46. Xu L, Zahid S, Khoshknab M, Moss J, Berger RD, Chrispin J *et al.* Conduction velocity dispersion predicts postinfarct ventricular tachycardia circuit sites and associates with Lipomatous Metaplasia. *J Am Coll Cardiol EP* 2023;**9**:1464–74.
47. Rajendran PS, Nakamura K, Ajijola OA, Vaseghi M, Armour JA, Ardell JL *et al.* Myocardial infarction induces structural and functional remodelling of the intrinsic cardiac nervous system. *J Physiol* 2016;**594**:321–41.
48. Szentandrássy N, Farkas V, Bárándi L, Hegyi B, Ruzsnavszky F, Horváth B *et al.* Role of action potential configuration and the contribution of Ca2+ and K+ currents to isoprenaline-induced changes in canine ventricular cells. *Br J Pharmacol* 2012;**167**:599–611.
49. Taggart P, Sutton P, Lab M, Dean J, Harrison F, Harrison JF *et al.* Interplay between Adrenaline and interbeat interval on ventricular repolarisation in intact heart in vivo. *Cardiovasc Res* 1990;**24**:884–95.
50. He B, Lu Z, He W, Wu L, Huang B, Yu L *et al.* Effects of low-intensity atrial ganglionated plexi stimulation on ventricular electrophysiology and arrhythmogenesis. *Auton Neurosci* 2013;**174**:54–60.